Biochimica et Biophysica Acta 1817 (2012) 672–679

Contents lists available at SciVerse ScienceDirect

Biochimica et Biophysica Acta

journal homepage: www.elsevier.com/locate/bbabio

Review

Kinetic studies of the reactions of O_2 and NO with reduced *Thermus thermophilus* ba_3 and bovine aa_3 using photolabile carriers ☆

Ólöf Einarsdóttir [a,*], Chie Funatogawa [a], Tewfik Soulimane [b,c], Istvan Szundi [a]

[a] Department of Chemistry and Biochemistry, University of California, Santa Cruz, CA 95064, USA
[b] Chemical and Environmental Sciences Department, University of Limerick, Ireland
[c] Materials and Surface Science Institute, University of Limerick, Ireland

ARTICLE INFO

Article history:
Received 11 September 2011
Received in revised form 8 December 2011
Accepted 8 December 2011
Available online 16 December 2011

Keywords:
Thermus thermophilus ba_3
O_2 and NO photolabile carriers
Double-laser transient absorption spectroscopy
CO photodissociation

ABSTRACT

The reactions of molecular oxygen (O_2) and nitric oxide (NO) with reduced *Thermus thermophilus* (*Tt*) ba_3 and bovine heart aa_3 were investigated by time-resolved optical absorption spectroscopy to establish possible relationships between the structural diversity of these enzymes and their reaction dynamics. To determine whether the photodissociated carbon monoxide (CO) in the CO flow-flash experiment affects the ligand binding dynamics, we monitored the reactions in the absence and presence of CO using photolabile O_2 and NO complexes. The binding of O_2/NO to reduced ba_3 in the absence of CO occurs with a second-order rate constant of $1\times10^9\ M^{-1}\ s^{-1}$. This rate is 10-times faster than for the mammalian enzyme, and which is attributed to structural differences in the ligand channels of the two enzymes. Moreover, the O_2/NO binding in ba_3 is 10-times slower in the presence of the photodissociated CO while the rates are the same for the bovine enzyme. This indicates that the photodissociated CO directly or indirectly impedes O_2 and NO access to the active site in *Tt* ba_3, and that traditional CO flow-flash experiments do not accurately reflect the O_2 and NO binding kinetics in ba_3. We suggest that in ba_3 the binding of O_2 (NO) to heme a_3^{2+} causes rapid dissociation of CO from Cu_B^+ through steric or electronic effects or, alternatively, that the photodissociated CO does not bind to Cu_B^+. These findings indicate that structural differences between *Tt* ba_3 and the bovine aa_3 enzyme are tightly linked to mechanistic differences in the functions of these enzymes. This article is part of a Special Issue entitled: Respiratory Oxidases.

1. Introduction

Activation of molecular oxygen and its four-electron reduction to water represent key processes of biological energy production in eukaryotes and many prokaryotes. The O_2 reduction is typically catalyzed by cytochrome and ubiquinol oxidases using electrons from respiratory electron transport [1–4]. This reaction is coupled to proton translocation across the inner mitochondrial or bacterial plasma membrane to generate an electrochemical proton gradient required for ATP synthesis [5].

Aside from the well known role of the heme–copper oxidases in energy conservation, cytochrome *c* oxidase is inhibited by nitric oxide (NO), and this inhibition has been implicated in the regulation of cellular respiration in eukaryotes [6,7]. Moreover, several bacterial heme–copper oxidases, including *Thermus thermophilus* (*Tt*) ba_3, *Escherichia coli* bo_3 ubiquinol oxidase and the cbb_3 oxidases, can catalyze the reduction of NO to nitrous oxide (N_2O), albeit with low efficiency [8–11]. NO denitrification by NO reductases (NORs) occurs in many prokaryotes and has been shown to endow various pathogenic bacteria with the ability to resist the mammalian immune response [12,13].

The mechanisms underlying the fast reactions of the heme–copper oxidases, O_2 activation, electron and proton transfer, and coupling of electron transfer to proton translocation, remain a major challenge in the field of bioenergetics. Crystallographic studies of the bovine enzyme and several bacterial oxidases have provided a detailed picture of the static structures of the enzymes [14–19]. While sequence homology of the catalytic subunit containing the active site binuclear center is high between the bovine enzyme and the bacterial *Rhodobacter sphaeroides* and *Paracoccus denitrificans* aa_3 oxidases (54 and 55%, respectively), it is much lower among other oxidases, including *Tt* ba_3 (23%). Considering the very different functional environments of *Tt* ba_3 and the bovine heart cytochrome oxidase, one might expect not only structural but also kinetic differences between the two enzymes. For instance, the significantly lower O_2 solubility at 70 °C, the optimum growth temperature of the *T. thermophilus* bacterium, compared to that at room temperature, argues for more efficient O_2 transport to the active site in *Tt* ba_3. However, applying the traditional CO flow-flash method to study the O_2 (and NO) binding dynamics in *Tt* ba_3 may be compromised by the fate of the photodissociated CO.

☆ This article is part of a Special Issue entitled: Respiratory Oxidases.

* Corresponding author. Tel.: +1 831 459 3155; fax: +1 831 459 2935.
E-mail address: olof@ucsc.edu (Ó. Einarsdóttir).

0005-2728/$ – see front matter © 2011 Elsevier B.V. All rights reserved.
doi:10.1016/j.bbabio.2011.12.005

Whether this is the case can only be addressed by directly comparing the binding of ligands such as O_2 and NO to *Tt* ba_3 and the aa_3 oxidases in the absence and presence of CO.

This paper summarizes recent investigations of NO binding and O_2 binding and reduction in *Tt* ba_3 and bovine aa_3 using a novel time-resolved spectroscopic approach based on photolabile O_2 and NO carriers. A comparative study of the two enzymes allows us to relate kinetic differences to their different structures, which evolved during adaptation to different physiological environments.

2. Ligand binding in the heme–copper oxidases

The ligand binding dynamics of O_2 and NO in the heme–copper oxidases are key elements of the physiological O_2 reduction, the NO inhibition of the mitochondrial enzyme, and the NO reductase activity of several of the bacterial oxidases. Carbon monoxide (CO), a competitive inhibitor of O_2 binding, has frequently been used to model O_2/NO binding in the heme–copper oxidases. Photodissociation and recombination studies of the CO-bound cytochrome oxidase dynamics have provided insights into the pathways of this ligand to and from heme a_3 at the active site [4,20]. Moreover, CO forms a thermodynamically and kinetically stable complex with the reduced high-spin heme, and photodissociation of CO from the heme in the presence of either O_2 or NO is generally used to initiate the reaction of these ligands with the reduced enzyme [21]. This "flow-flash" approach circumvents the rate limitation of conventional mixing techniques and has been used extensively to investigate O_2 binding and reduction on time scales from microseconds to milliseconds [1–4].

The success of the CO flow-flash technique is contingent on the photodissociated CO not interfering with O_2 or NO binding at the binuclear center. Low-temperature Fourier transform infrared (FTIR) and time-resolved infrared (TRIR) studies have shown that the photodissociated CO binds to Cu_B^+ in several heme–copper oxidases, including the mitochondrial aa_3 [22–24] and *Tt* ba_3 [25,26]. The pathway of CO from the solution to its binding site on heme a_3^{2+} has likewise been proposed to involve a $Cu_B^+ - CO$ intermediate [23,24], with Cu_B^+ acting as a gateway for transporting CO and, by inference, other ligands such as NO and O_2 to and from the reduced high-spin heme a_3 [24,27]. In the mitochondrial enzyme, the $Cu_B^+ - CO$ photoproduct decays with a lifetime of ~1.5 μs [23,24], while in *Tt* ba_3, the reported lifetime is ~30 ms [26]. The long lifetime of the $Cu_B^+ - CO$ complex in ba_3 raises questions whether the O_2/NO binding to heme a_3^{2+} is impeded by the photodissociated CO in CO flow-flash experiments on this enzyme, and, secondly, whether the binding of these ligands to heme a_3^{2+} in ba_3, and possibly other heme–copper oxidases, is in fact preceded by binding to Cu_B^+. The fate of the photodissociated CO is also significant with respect to establishing whether two ligands can be accommodated simultaneously at the active site. This is of particular relevance for the bacterial heme–copper oxidases with NO reductase activity, which requires at least the transient presence of two NO molecules at the active site [28]. Ultrafast transient absorption measurements of the photolyzed NO-bound bovine aa_3, *P. denitrificans* aa_3 and *Tt* ba_3 have provided important insight into the NO recombination dynamics of these enzymes on a fast time scale [27–29]. However, kinetic studies of the direct binding of NO from solution to reduced ba_3 and the effect of CO on the NO binding dynamics have not been undertaken.

To address these issues, we investigated the reactions of O_2/NO with reduced *Tt* ba_3 and the bovine cytochrome oxidase at room temperature using photolabile O_2 and NO carriers (see Supporting Information for experimental details). This method eliminates the interference from the photodissociated CO in the CO flow-flash method and circumvents the low NO quantum yield in NO flash-photolysis studies and the rate-limitation of traditional NO stopped-flow methods. Both the photolabile O_2 complex, $[(\mu\text{-}O_2)(\mu\text{-}OH)(Co(bpy)_2)_2]^{3+}$, and the NO-complex, $K_2RuNOCl_5$, are stable under anaerobic conditions at pH 7 and release O_2 or NO within the 7 ns 355 nm laser pulse (this study and [30,31]). Moreover, neither the complexes nor their respective photoproducts react with the enzymes during the transient absorption measurements. By exploring the binding of both O_2 and NO to the reduced enzymes, we can probe the microsecond time scale ligand binding dynamics during the physiological O_2 reduction as well as in the absence of redox chemistry (NO). We also monitored the O_2 reduction in ba_3 and extracted the absorption spectra of the respective intermediates based upon proposed mechanisms (these studies will be discussed in Section 3 on the O_2 reduction mechanism). For comparison, we investigated the reactions of O_2 and NO with both *Tt* ba_3 and bovine aa_3 using a double-laser approach in which the fully reduced CO-bound enzymes were photolyzed with a 532 nm laser pulse and O_2 or NO was generated simultaneously by photolyzing the respective photolabile carrier with a 355 nm laser pulse [32]. This approach, unlike the CO flow-flash method, is not limited to enzymes with strong binding of CO to heme a_3^{2+}.

2.1. NO binding to reduced *Tt* ba_3 and bovine aa_3

Fig. 1 (a and b) shows the time-resolved optical absorption difference spectra (post-minus pre-photolysis) recorded during the reaction of reduced ba_3 with photoproduced NO in the absence and presence of CO, respectively. In the presence of CO, the reduced CO-bound enzyme was photolyzed with a 532 nm laser pulse and NO was generated simultaneously with a 355 nm laser flash. The corresponding difference spectra for the bovine enzyme are shown in Fig. 2a and b, respectively.

The effect of CO on the rate of NO binding to reduced ba_3 can be clearly visualized when the time dependence of the absorbance is plotted at a specific wavelength. Fig. 3a shows a comparison between the NO binding kinetics for ba_3 at 444 nm, the absorption maximum of the reduced heme a_3, in the absence (open circles) and presence of CO (closed circles). Fig. 3b demonstrates analogous traces for the bovine enzyme in the absence and presence of CO (open and closed triangles, respectively). The data are extracted from Figs. 1 and 2, and the solid lines represent absorbance changes calculated on the basis of global exponential fits to the data (see below). It is clear that the binding of NO to reduced ba_3 is significantly faster in the absence of CO (Fig. 3a), while the rates are the same for the bovine enzyme (Fig. 3b).

The time-resolved difference spectra were subjected to singular value decomposition (SVD) and global exponential fitting [33–36]. A single apparent lifetime of 16 μs (60 μM NO) was observed for ba_3 in the absence of CO. This process is attributed to NO binding to heme a_3^{2+} based on the corresponding spectral change, represented by the *b*-spectrum (Fig. 4a, solid curve). In the case of a single-step mechanism, the *b*-spectrum is the difference between the spectra of the first and second intermediates, i.e. the reduced and NO-bound enzymes, respectively. The time-independent b_o-spectrum (dashed curve) is the difference spectrum at infinite time. The 16 μs lifetime at 60 μM NO concentration corresponds to a second-order rate constant of $1\times10^9\ M^{-1}\ s^{-1}$ for NO binding to reduced ba_3 in the absence of CO. The value of the second-order rate constant and the linearity of the binding rate with NO concentration were confirmed using different NO concentrations (Fig. S1).

SVD-based global exponential fitting of the time-resolved difference spectra recorded during the reaction of reduced ba_3 with NO in the presence of CO revealed an apparent lifetime of 166 μs at 70 μM NO concentration. This corresponds to a second-order rate constant for NO binding of $9\times10^7\ M^{-1}\ s^{-1}$, a rate ~10-times slower than in the absence of CO. The respective spectral change is shown in Fig. 4b (solid curve); the dashed line represents the time-independent b_0-spectrum.

For the bovine enzyme, apparent lifetimes of 127 μs (87 μM NO) and 105 μs (105 μM NO) were observed in the absence and presence

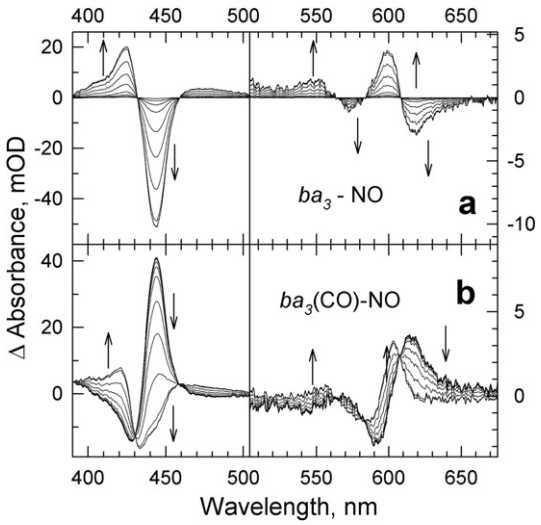

Fig. 1. Time-resolved optical absorption difference spectra (post-minus pre-photolysis) of the reaction of the fully reduced *Tt* ba_3 with photoproduced NO in the absence of CO (panel a) and the presence of CO (panel b). The spectra were obtained by subtracting the spectral contribution of the photolyzed NO complex, determined in a separate experiment. The spectra (SVD-filtered) were recorded at 12–16 delay times, equally spaced on a logarithmic scale, between 200 ns–10 ms in the absence of CO and 500 ns–50 ms in the presence of CO. The arrows represent the direction of the absorbance change with time. Conditions: the effective enzyme concentration, 1.2 μM; 0.1 M HEPES (pH 7.5); 0.1% DM; effective NO concentration, 60 μM (panel a) and 70 μM (panel b); optical path, 0.5 cm. The CO concentration was 0.5 mM after mixing.

of CO, respectively, with *b*-spectra analogous to those observed for the *Tt* ba_3. These lifetimes correspond to the same second-order rate constant, $9\times10^7\ M^{-1}\ s^{-1}$, in the absence and presence of CO.

2.2. O_2 binding to Tt ba_3 and bovine aa_3

Our laboratory recently investigated the O_2 binding and reduction in *Tt* ba_3 in the absence and presence of CO using a photolabile O_2 carrier [32]. SVD-based global exponential fitting and kinetic analysis of the time-resolved data recorded during the O_2 reduction by ba_3 showed that the O_2 binding at 90 μM O_2 concentration occurs with

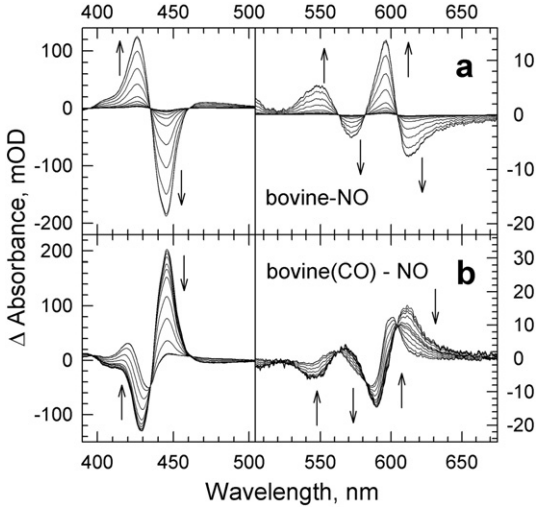

Fig. 2. Time-resolved optical absorption difference spectra for the reaction of the fully reduced bovine aa_3 with photoproduced NO in the absence of CO (panel a; 100 ns–10 ms) and the presence of CO (panel b; 200 ns–10 ms) (see Fig. 1 for details). Conditions: the effective enzyme concentration, 5.2 μM; 50 mM Na-phosphate (pH 7.5); effective NO concentration: 87 μM (a) and 105 μM (b). The CO concentration was 0.5 mM after mixing.

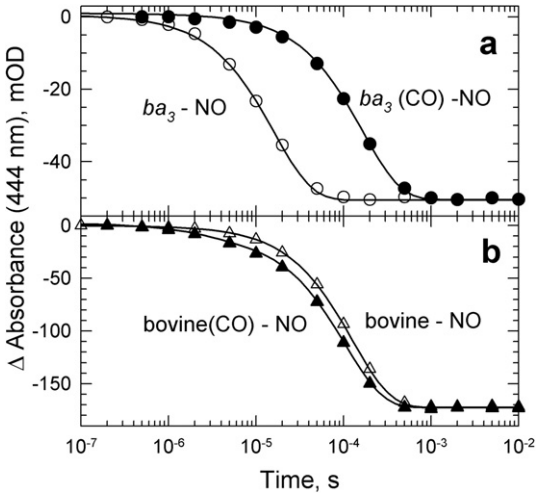

Fig. 3. Comparison of the transient absorbance changes taking place at 444 nm during the reaction of fully reduced *Tt* ba_3 (panel a) and bovine aa_3 (panel b) with photoproduced NO in the presence of CO (filled circles and triangles) and in the absence of CO (open circles and triangles). The kinetic traces in panels a and b are from the time-resolved data in Figs. 1 and 2, respectively, and are normalized to the total absorbance change. The solid lines represent the absorbance traces at 444 nm, calculated on the basis of the global exponential fits (see text for details).

an apparent lifetime of 9.3 μs in the absence of CO and 110 μs in the presence of CO. This corresponds to second-order rate constants of 1×10^9 and $1\times10^8\ M^{-1}\ s^{-1}$, respectively; the details of the kinetic analysis are discussed in Ref. [32] and in Section 3 on the O_2 reduction mechanism. The rate of O_2 binding in the bovine enzyme was the same in the absence and presence of CO, $\sim1\times10^8\ M^{-1}\ s^{-1}$.

Our results demonstrate that in the absence of CO, the rate of O_2 and NO binding to heme a_3^{2+} in ba_3, $1\times10^9\ M^{-1}\ s^{-1}$, approaches the diffusion-controlled limit and is 10-fold faster than in the presence of photodissociated CO. In contrast, the rate of either O_2 or NO binding to heme a_3^{2+} in the bovine enzyme is the same in the presence and absence of CO. These results indicate different ligand accessibility in *Tt* ba_3 and the bovine enzyme, and suggest that in ba_3 the presence of CO on Cu_B^+ or at a nearby docking site impedes the access of O_2/NO to the heme a_3 site; the different possibilities will be discussed below. Our studies also show that for *Tt* ba_3, the CO flow-flash method does not give accurate results for the "physiological" O_2 and NO binding kinetics, namely, that observed in the absence of CO.

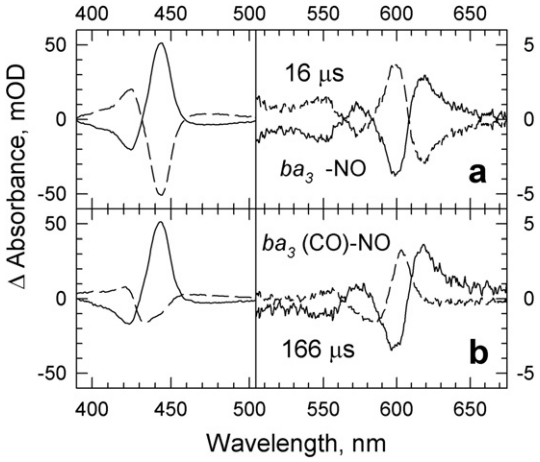

Fig. 4. The spectral amplitudes (*b*-spectra; solid curves) and lifetimes from a global-exponential fit to the time-resolved data recorded during the reaction of NO with reduced *Tt* ba_3 in the absence (a) and presence (b) of CO. The time-independent b_o-spectra (dashed curves) represent the difference spectra extrapolated to infinite time, namely, the difference between the spectra of the NO-bound and reduced enzymes (a), and the NO-bound and CO-bound enzymes (b).

2.3. Does Cu_B^+ act as an obligatory way-station for ligand binding to heme a_3?

Our observations have important implications and raise several questions regarding the possible mechanisms of ligand binding at the binuclear center in *Tt* ba_3. One question concerns whether the binding of O_2/NO to Cu_B^+ on route to and from heme a_3^{2+} is indeed a common mechanistic feature among the different oxidases as proposed for CO [20]. In ba_3, the rate of O_2/NO binding to heme a_3^{2+} in the absence of CO is close to the diffusion-controlled limit. Therefore, if O_2/NO binds to Cu_B^+ on its route to heme a_3, this binding does not appear to limit the approach of the ligands to heme a_3^{2+} to any significant extent. Carbon monoxide has been reported to bind to Cu_B^+ in the bovine enzyme with an upper limit of 1 ps following photolysis of CO from heme a_3^{2+} [37]. Thus, by inference, the photodissociated CO would be expected to bind to Cu_B^+ in ba_3 much faster than the photoproduced O_2/NO. The reported affinity of Cu_B^+ for NO is also much lower than that for CO [9], and thus NO is unlikely to replace CO at the Cu_B^+ site. The affinity of the reduced Cu_B for CO would also be expected to be significantly higher than that of O_2. Therefore, if the photodissociated CO stays bound to Cu_B^+ in ba_3 for hundreds of microseconds, Cu_B could not be an obligatory way-station for O_2/NO binding to heme a_3^{2+}.

2.4. Does the reduced binuclear center in Tt ba_3 bind one or two ligands simultaneously?

The above discussion raises a fundamental question whether the active site of reduced *Tt* ba_3 can accommodate the simultaneous binding of two ligand molecules, one on heme a_3 and the other on Cu_B. Low-temperature EPR and room temperature optical studies of the NO binding dynamics of reduced ba_3 and *P. denitrificans* aa_3 concluded that only one NO was bound with high affinity to heme a_3^{2+} in ba_3 whereas two NO molecules could bind at the active site of the *Paracoccus* enzyme, one at heme a_3^{2+} and the other presumably at Cu_B^+; the binding of a second molecule in ba_3 with low affinity was not excluded [28]. Low-temperature (30 K) FTIR experiments indicated that the reduced *E. coli* bo_3, which like *Tt* ba_3, reduces NO to N_2O [8], simultaneously binds NO and CO to the reduced high-spin heme and Cu_B, respectively, while *Thermus* ba_3 does not [38]. This difference was attributed to the greater distance between Cu_B and the heme a_3 iron in the bo_3 oxidase (5.30 Å) compared to that in ba_3 (4.4–4.7 Å) [14,17,39]; these distances refer X-ray data of the oxidized enzymes. The shorter iron–copper distance in ba_3 suggests that the simultaneous binding of CO to Cu_B^+ and either O_2 or NO to heme a_3^{2+} would likely require significant conformational changes at the active site. Recent crystallographic studies have indicated that the reduction of ba_3 increases the distance between heme a_3^{2+} and Cu_B^+ by 0.3 Å, with the concomitant loss of a H_2O molecule between the two metal centers [40]; these redox-induced conformational changes at the active site are likely to be of mechanistic importance for O_2/NO binding and reduction. It should also be noted that in ba_3, the high-spin heme a_3 is tilted away from Cu_B, making the surface area of the binuclear center that is presented to an approaching ligand larger than in the aa_3 oxidases. With regards to the NO reductase activity of ba_3, this might allow a "second" NO molecule to react with NO already bound to the high-spin heme. Based on theoretical studies of the NO reductase activity in ba_3, Blomberg and coworkers proposed a reaction mechanism in which the binding of the first NO molecule to heme a_3^{2+} activates the attack of a second NO molecule, generating a cyclic hyponitrous acid anhydride intermediate with the two oxygens coordinating to Cu_B^+ [41].

2.5. How does CO impede ligand access to the active site in Tt ba_3?

If CO remains on Cu_B^+ for milliseconds and the binuclear center of ba_3 is only able to accommodate one ligand, then the rapid binding of O_2/NO would not be expected to occur. This is clearly not the case. This raises questions whether the photodissociated CO does indeed bind to Cu_B^+ and whether the infrared frequency observed at 2053 cm^{-1} following photolysis of the CO-bound ba_3 arises from CO bound to Cu_B^+ [25,26] or from CO being trapped at "docking" site [42]. Interestingly, FTIR studies of the signal transducer O_2-sensing protein HemAT, a heme protein lacking copper, revealed a well-defined peak at 2065 cm^{-1} in the spectrum of the equilibrium CO-bound sensor and in its light-minus-dark FTIR difference spectrum [43]. A recent crystal structure of the bovine aa_3-CO shows that CO binds to Cu_B^+ in a side-on fashion after photolysis of CO from heme a_3^{2+}. The Cu_B^+-to-carbon and Cu_B^+-to-oxygen atom distances of 2.4 and 2.7 Å, respectively, indicate a very weak Cu_B^+ – CO bond [44,45]. Significantly, no infrared linear dichroism was observed for the transient photoproduct of the CO-bound bovine aa_3, which was interpreted in terms of CO being bound to Cu_B^+ at the "magic angle" to the heme normal [46]; another explanation is that the photodissociated CO does not bind to Cu_B^+. If the latter is the case for ba_3, the presence of CO at a "docking site" [42] may impede the access of O_2/NO to heme a_3^{2+}, resulting in the 10-fold difference in the ligand binding rate between the reduced ba_3 and the CO-photolyzed reduced ba_3.

Alternatively, the binding of the photodissociated CO to Cu_B^+ may directly impede O_2/NO access to heme in ba_3. If the simultaneous binding of CO to Cu_B^+ and O_2/NO to heme a_3^{2+} does occur, and if CO remains bound to Cu_B^+ for longer than a few microseconds, Cu_B^+ would be unable to act as an electron donor for the rapid O – O bond cleavage (4–5 μs) in ba_3 (see below and Ref. [32]). However, the binding of O_2 to heme a_3^{2+} and the driving force for the subsequent O – O bond cleavage may cause a change in the tetrahedral geometry of Cu_B^+ toward more square planar, which would facilitate the oxidation of Cu_B^+ and the dissociation of CO from Cu_B^+. The observation that in ba_3 the 5 μs rate of O – O bond cleavage is the same in the absence (see below and Ref. [32]) and presence of CO [47], suggests that the CO dissociation from Cu_B^+ is not the rate-limiting step for the electron transfer to the bound dioxygen. In the bovine enzyme, the CO dissociates from Cu_B^+ on a time scale of 1.5 μs [23,24], rapidly enough not to interfere with the binding of O_2/NO to heme a_3^{2+}.

The slower O_2/NO binding to heme a_3^{2+} in ba_3 in the presence of CO may also arise because the reduced enzyme generated after CO photodissociation has a conformation less favorable for ligand access to heme a_3^{2+} than the normal reduced enzyme. A "global" structural change at the active site of ba_3 as a result of ligand binding to heme a_3^{2+} is supported by time-resolved magnetic circular dichroism and circular dichroism photolysis experiments of the fully reduced CO-bound ba_3 [48]. These measurements showed that the high-spin photoproduced heme a_3^{2+} is spectrally distinct from that observed for the steady-state reduced ba_3. These spectral differences were interpreted in terms of a small but global conformational change in the protein upon CO binding to heme a_3^{2+}, persisting after the Fe–CO photodissociation [48].

2.6. Ligand binding in Tt ba_3 versus bovine aa_3

The binding of O_2 and NO to heme a_3^{2+} in ba_3 in the absence of CO is 10-times faster than the binding of these ligands to the bovine enzyme under similar conditions. We attribute the order of magnitude difference in the ligand binding rates to structural variations in the dioxygen channel of the two enzymes, with a more open ligand access in ba_3. In the bovine enzyme, as well as *R. sphaeroides* and *P. denitrificans* aa_3, a constriction point reduces the diameter of the O_2 channel, which likely impedes the access of ligands to heme a_3 [49,50]. These structural differences in the O_2 channel may be related to the functional requirements of the two enzymes, with the *Thermus* enzyme operating optimally at 70 °C, at which temperature the O_2 solubility is about half of that in water at 25 °C [32,49]. Further

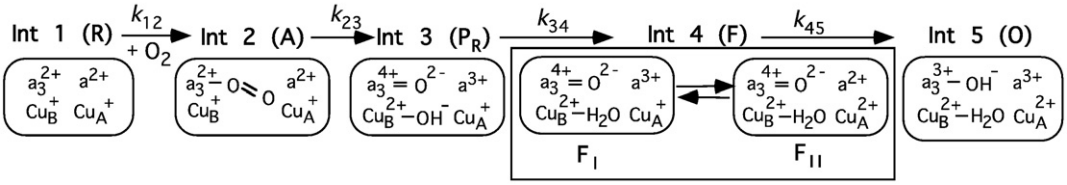

Scheme 1. The conventional sequential unidirectional mechanism for the reduction of dioxygen to water.

understanding of the structural features controlling ligand (O_2, NO and CO) binding dynamics and reactivities of the different oxidase families will provide insight into the function of these enzymes and how the protein scaffold tunes ligand pathways for different physiological environments.

3. The O_2 reduction mechanism in the heme–copper oxidases

The reduction of O_2 to water in the heme–copper oxidases takes place at the Cu_B and the high-spin heme (a_3, b_3, o_3); a low-spin heme serves as the electron donor to the binuclear center. Kinetic studies of the O_2 reduction have generally relied on the CO flow-flash technique, with the primary focus on the mitochondrial and the A-type bacterial oxidases [1–4]. Less emphasis has, until recently, been placed on the B-type oxidases, including the *Thermus* ba_3 enzyme [32,47,51,52]. Most of these transient optical measurements are based on single-wavelength detection in which the O_2 kinetics and corresponding spectral changes are recorded at a few selected wavelengths. Because of the limited spectral information, it is difficult to derive a detailed kinetic picture using this technique. The O_2 reduction kinetics has generally been interpreted in terms of a unidirectional sequential mechanism (Scheme 1), with decreasing values of the apparent rate constants assigned to consecutive steps. However, recent studies in our laboratory using multi-wavelength detection and advanced data analysis have raised questions about these conventional rate assignments in *Tt* ba_3. These studies are summarized below.

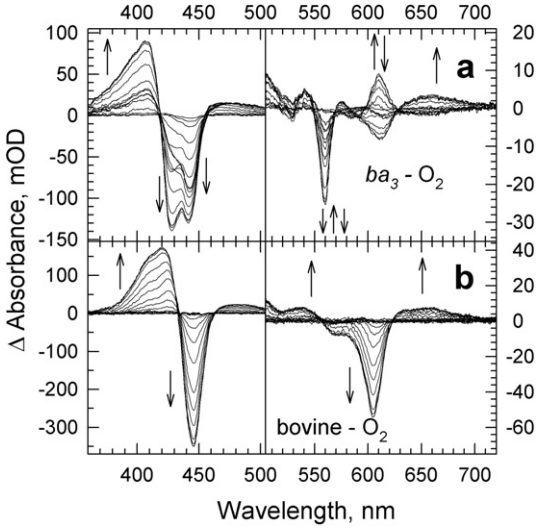

Fig. 5. Time-resolved optical absorption difference spectra (post-minus pre-photolysis) recorded during the reaction of dioxygen with the fully reduced *Tt* ba_3 (panel a) and bovine enzyme (panel b) in the absence of CO. The spectra are those obtained after subtracting the spectral contribution of the photolyzed O_2 complex, determined in a separate experiment. The spectra (SVD-filtered) were recorded at 15–17 delay times, equally spaced on a logarithmic scale, between 500 ns–20 ms (panel a) and 200 ns–50 ms (panel b). The arrows represent the direction of the absorbance change with time. Conditions: ba_3: 0.1 M HEPES (pH 7.5); 0.1% DM; effective enzyme concentration, 2.6 μM; bovine enzyme: 50 m N NaPi (pH 7.5) effective enzyme concentration, 4.3 μM; optical path, 0.5 cm.

3.1. The reaction of reduced *Tt* ba_3 with O_2 in the absence of CO

To investigate the applicability of the conventional sequential O_2 reduction mechanism (Scheme 1) to the different heme–copper oxidases, we investigated the reactions of the reduced *Tt* ba_3 and the bovine heart enzyme with photoproduced O_2 in the absence of CO (see Supporting Information and Ref. [32] for experimental details). The time-resolved difference spectra are shown in Fig. 5a and b, respectively. The difference spectra were analyzed using SVD and global exponential fitting. The time dependence of the spectra recorded during the reaction of reduced ba_3 with O_2 (90 μM O_2) in the absence of CO was best fitted with four apparent lifetimes, 4.8 μs, 9.3 μs, 55 μs and 1.0 ms. Fig. 6a (solid lines) shows the intermediate spectra (referenced versus the reduced ba_3) extracted based on a fast–slow sequential mechanism in which decreasing values of the apparent rate constants (increasing lifetimes) are assigned to consecutive steps (Scheme 2). Fig. 6b shows the corresponding model spectra generated from the linear combination of the ground state model spectra; the model difference spectrum of compound **A** is that of the bovine enzyme.

When the data were analyzed in terms of this traditional "fast–slow" mechanism, the difference spectrum of compound **A** (Fig. 6a, green solid curve) had the same shape as the corresponding difference spectrum of the bovine enzyme (Fig. 6b, green curve) but with half the amplitude. This discrepancy was also noted in previous fast-mixing CO flow-flash studies on ba_3 [47]. Using a kinetic analysis based on the apparent rates and *b*-spectra, we were able exclude the reversibility of dioxygen binding as being the source of the reduced amplitude of the compound **A** spectrum [32]. A correspondence between the experimental and model spectra of compound **A** was attained only when the data were analyzed using a mechanism in which the 9.3 μs lifetime for O_2 binding was followed by the shorter 4.8 μs lifetime of O – O bond cleavage (Scheme 3). The green dashed curve in Fig. 6a shows the increased amplitude of the spectrum of compound **A** extracted using this slow–fast mechanism. The increased amplitude is in excellent agreement with the expected amplitude (Fig. 6b, green curve). The 9.3 μs lifetime at 90 μM O_2 concentration corresponds to a second-order rate constant of $1\times10^9\ M^{-1}\ s^{-1}$, which is 10-times faster than observed for the bovine enzyme. Repeating the experiment at half the O_2 concentration (45 μM) increased the 9.3 μs lifetime to 18 μs while the 4.8 μs lifetime was unchanged. This observation supports the assignment of the 9.3 μs process to O_2 binding [32]. The rate constant of $1\times10^9\ M^{-1}\ s^{-1}$ is the same as we observed for NO binding to heme a_3^{2+} in ba_3 in the absence of CO, further supporting the assignment of the 9.3 μs lifetime to the O_2-binding step.

There is an interesting parallel between a slow–fast mechanism and a mechanism containing a reversible step followed by an irreversible one; this can be demonstrated using the algebraic kinetic analysis method [32]. Both of these physical mechanisms produce very similar experimental data. When these data are analyzed by

$$\mathbf{R} \xrightarrow{4.8\ \mu s} \mathbf{A} \xrightarrow{9.3\ \mu s} \mathbf{P_I} \xrightarrow{55\ \mu s} \mathbf{P_{II}} \xrightarrow{1.0\ ms} \mathbf{O}$$

Scheme 2. A unidirectional "fast–slow" sequential mechanism of O_2 reduction for ba_3 in the absence of CO.

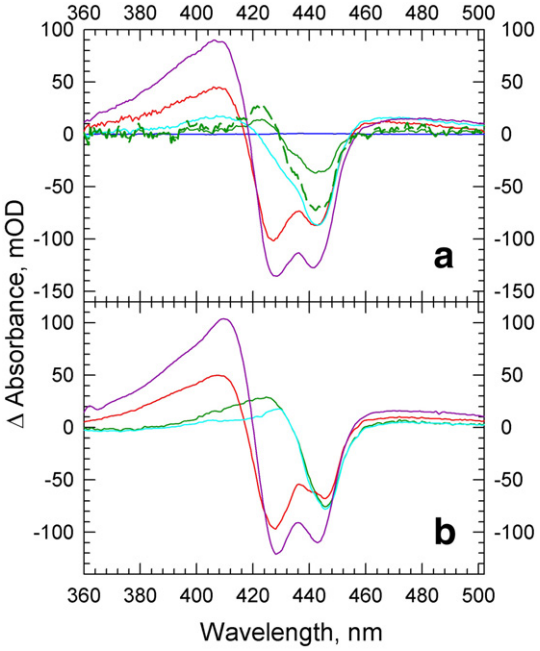

Fig. 6. (Panel a) (Solid lines) The experimental intermediate spectra (referenced versus the reduced enzyme) for the reaction of reduced *Tt* ba_3 with O_2 in the absence of CO. The spectra were extracted on the basis of the fast–slow mechanism in Scheme 2: compound **A** (green), $\mathbf{P_I}$ (red), $\mathbf{P_{II}}$ (cyan) and **O** (magenta). The spectrum of Int 2 extracted using the fast–slow Scheme 2 has the shape of compound **A** of the bovine heart oxidase but significantly lower amplitude. (Dashed, green curve) The spectrum of compound **A** extracted using the slow–fast mechanism in Scheme 3, in which the 9.3 μs process is followed by the 4.8 μs step. (Panel b) The model spectra of the proposed intermediates, compound **A** (green), $\mathbf{P_I}$ (red), $\mathbf{P_{II}}$ (cyan) and **O** (magenta), were generated based on the linear combinations of the ground-state spectra of ba_3; the difference spectrum of compound **A** is that of the bovine enzyme. The spectra in panel a are normalized to the enzyme concentration in panel b.

the traditional fast–slow scheme, the spectrum of the second intermediate in the scheme appears to be a mixture of the spectra of the first and second intermediates of the true mechanism [32]. However, a combination of multi-wavelength detection and quantitative kinetic analysis can distinguish between the two choices and identify the most probable underlying mechanism [32]. It should be noted that the 9.3 μs lifetime at 90 μM O_2 concentration corresponds to an apparent lifetime of ~1 μs at 1 mM O_2, at which concentration the reaction would indeed follow a mechanism with increasing lifetimes assigned to consecutive steps. However, at lower O_2 concentrations (~100 μM O_2) in the absence of CO [32] or when using the CO flow-flash method at 1 mM O_2 the slower O_2 binding, ~10 μs in both cases, would be followed by the faster 5 μs O – O bond cleavage.

The third and fourth intermediates (Fig. 6a, red and cyan, respectively) generated during O_2 reduction in ba_3, both correspond to **P** but with heme *b* oxidized in the former ($\mathbf{P_I}$) and rereduced in the latter ($\mathbf{P_{II}}$) (Scheme 3); no 580-nm oxyferryl **F** form is observed, in agreement with recent CO flow-flash experiments on ba_3 [47,52]. The $\mathbf{P_I}$ intermediate formed upon the decay of compound **A** (Fig. 6a, red curve) is well modeled by the $\mathbf{P_M}$ spectrum of ba_3 (heme *b* oxidized) (Fig. 6b, red curve). In contrast, the spectrum of $\mathbf{P_R}$ of the bovine enzyme, extracted from the time-resolved data obtained in a traditional CO flow-flash

$$\mathbf{R} \xrightarrow{9.3\ \mu s} \mathbf{A} \xrightarrow{4.8\ \mu s} \mathbf{P_I} \xrightarrow{55\ \mu s} \mathbf{P_{II}} \xrightarrow{1.0\ ms} \mathbf{O}$$

Scheme 3. The "slow–fast" sequential mechanism for the reaction of ba_3 with photoproduced O_2 in the absence of CO.

experiment, is considerably broader in the visible region than that of $\mathbf{P_I}$ for ba_3 [53]. These observations support that $\mathbf{P_R}$ in the bovine enzyme and $\mathbf{P_I}$ in ba_3 are indeed spectrally different. Our previous studies show that $\mathbf{P_R}$ is best modeled by a mixture of the spectra of compound **A**, **P** and **F**, which we interpreted in terms of a branched mechanism [36,54].

3.2. The reaction of reduced Tt ba_3 with O_2 in the presence of CO

The reaction of reduced ba_3 with O_2 in the presence of CO was initiated by simultaneously photolyzing the fully reduced CO-bound enzyme and the photolabile O_2 complex with 532 and 355 nm laser pulses, respectively [32]. In the presence of CO, three apparent lifetimes, 59 μs, 110 μs and 0.82 ms, were resolved for the reaction of O_2 with ba_3 at 90 μM O_2 concentration. Kinetic analysis based on the apparent rates and the corresponding spectral changes (*b*-spectra), together with a comparison of the extracted intermediate spectra with model spectra, showed that the 110 μs lifetime is due to O_2 binding, followed by the O – O bond cleavage on 5 μs time scale (**A** to $\mathbf{P_I}$) [32]; the latter process is not resolved in our experiment due to the rate-limiting nature of the O_2-binding step. The generation of $\mathbf{P_I}$ is followed by the formation of $\mathbf{P_{II}}$ (59 μs) and the subsequent generation of the oxidized enzyme (0.82 ms).

3.3. The reaction of O_2 with the reduced bovine heart oxidase in the absence of CO

The reaction of the reduced bovine heart enzyme with dioxygen was investigated in the absence of CO using the photolabile O_2 carrier. SVD-based global exponential fitting of the time-resolved difference spectra resolved four lifetimes, 42 μs, 160 μs, 1.1 ms and 4.3 ms at 70 μM O_2 concentration. Kinetic analysis similar to that applied to the ba_3 showed that the 160 μs lifetime represents the binding of O_2 to heme a_3^{2+}. This lifetime corresponds to a second-order rate constant of O_2 binding of $\sim 1\times10^8\ M^{-1}\ s^{-1}$, which is equivalent to that observed in CO flow-flash experiments [55–57]. The 42 μs lifetime is the result of heme *a* oxidation, a dominant spectral change following O_2 binding. However, the individual formation of $\mathbf{P_R}$ and $\mathbf{F_I}$/$\mathbf{F_{II}}$ was not resolved because both processes are faster than the O_2-binding step. Both millisecond processes show spectral changes characteristic of the final oxidation step [36].

3.4. Comparison of the early kinetic steps in Tt ba_3 and bovine aa_3

In addition to the 10-times faster O_2/NO binding in ba_3 compared to the bovine enzyme, the conversion of compound **A** to $\mathbf{P_I}$ is ~8 times faster in ba_3 (4.8 μs compared to ~40 μs in the bovine enzyme). This may be due to different redox potentials of the high- and low-spin hemes in the two enzymes. The absence of electron back-flow following photolysis of the mixed-valence CO-bound ba_3 is in line with this suggestion (unpublished results). A relatively short heme a_3 iron-Cu_B distance in ba_3 may also facilitate electron transfer from Cu_B^+ to the oxygen-bound heme a_3.

Our results show that following the decay of compound **A** in ba_3 to $\mathbf{P_I}$, the subsequent reduction of the oxidized heme *b* is not associated with the formation of the 580-nm oxyferryl **F** intermediate, as in the bovine enzyme, but instead the generation of an intermediate which maintains the spectral signature of **P** ($\mathbf{P_{II}}$). This observation is in agreement with recent CO flow-flash results on ba_3 [47,52]. Thus despite similarities between the bovine enzyme and *Thermus* ba_3 at the active site, there are sufficient structural and dynamic differences to produce different intermediates in the two enzymes. As previously suggested, the proton acceptor postulated to cause the spectral differences between **P** and **F**, i.e. the deprotonated cross-linked tyrosine, $Y244^-$, or Cu_B^+-OH^-, may be different in the two enzymes [47,52].

4. Conclusions

Several important conclusions can be drawn from our studies. First, the results show superfast O_2 and NO binding to reduced ba_3 in the absence of CO, with the rates of O_2 and NO binding approaching the diffusion-controlled limit. These rates are 10-times greater than found for ba_3 in the presence of CO, indicating that the photodissociated CO directly or indirectly impedes O_2 and NO access to the active site in this enzyme. Therefore, the CO flow-flash approach does not accurately reflect the O_2 and NO binding kinetics in ba_3. Second, our kinetic analysis demonstrates that the breaking of the O – O bond occurs on ~5 μs time scale, 8-times faster than in the bovine enzyme. Third, our results show that the binding of O_2 and NO to heme a_3^{2+} in ba_3 in the absence of the photodissociated CO is 10-times faster than in the bovine enzyme under equivalent conditions or when using the CO flow-flash method. Together these results indicate important structural differences between the accessibility of O_2/NO to the active site in ba_3 and the bovine heart enzyme. We suggest that the different ligand access is related to a constriction point in the oxygen channel of the aa_3 oxidases, which is not present in ba_3 [49].

The fast rates of O_2 and NO binding to heme a_3^{2+} in ba_3 in both the absence and presence of CO and the reported long lifetime of the Cu_B^+ – CO complex suggest that Cu_B^+ may not act as a gateway for O_2/NO binding to heme a_3^{2+} in ba_3. Our findings also raise a fundamental question about whether the photodissociated CO impedes the access of O_2/NO to heme a_3^{2+}, either by binding to Cu_B^+ or being present at ligand docking site. If the former is true, we propose that during the CO flow-flash method, or when using the double-laser approach, the O_2 binding to heme a_3^{2+} causes CO to dissociate from Cu_B^+ through steric and electronic effects, thereby allowing Cu_B^+ to act as an electron donor during O – O bond cleavage.

Supplementary materials related to this article can be found online at doi:10.1016/j.bbabio.2011.12.005.

Acknowledgements

This work was supported by the National Institutes of Health Grants GM 53788 (OE) and the Science Foundation Ireland (BICF685 to TS). We thank Dr. James A. Fee, Dept. of Molecular Biology, The Scripps Institute, for providing *Thermus thermophilus* ba_3 for preliminary O_2 reduction experiments and for helpful discussions. We thank Dr. William McDonald for helpful discussions.

References

[1] P. Brzezinski, G. Larsson, Redox-driven proton pumping by heme–copper oxidases, Biochim. Biophys. Acta 1605 (2003) 1–13.
[2] S. Ferguson-Miller, G.T. Babcock, Heme/copper terminal oxidases, Chem. Rev. 96 (1996) 2889–2907.
[3] V.R. Kaila, M.I. Verkhovsky, M. Wikström, Proton-coupled electron transfer in cytochrome oxidase, Chem. Rev. 110 (2010) 7062–7081.
[4] Ó. Einarsdóttir, Fast reactions of cytochrome oxidase, Biochim. Biophys. Acta 1229 (1995) 129–147.
[5] M.K.F. Wikström, Proton pump coupled to cytochrome *c* oxidase in mitochondria, Nature 266 (1977) 271–273.
[6] C.E. Cooper, G.C. Brown, The inhibition of mitochondrial cytochrome oxidase by the gases carbon monoxide, nitric oxide, hydrogen cyanide and hydrogen sulfide: chemical mechanism and physiological significance, J. Bioenerg. Biomembr. 40 (2008) 533–539.
[7] M.G. Mason, P. Nicholls, M.T. Wilson, C.E. Cooper, Nitric oxide inhibition of respiration involves both competitive (heme) and noncompetitive (copper) binding to cytochrome *c* oxidase, Proc. Natl. Acad. Sci. U. S. A. 103 (2006) 708–713.
[8] C.S. Butler, E. Forte, F.M. Scandurra, M. Arese, A. Giuffrè, C. Greenwood, P. Sarti, Cytochrome bo_3 from *Escherichia coli*: the binding and turnover of nitric oxide, Biochem. Biophys. Res. Commun. 296 (2002) 1272–1278.
[9] A. Giuffrè, G. Stubauer, P. Sarti, M. Brunori, W.G. Zumft, G. Buse, T. Soulimane, The heme–copper oxidases of *Thermus thermophilus* catalyze the reduction of nitric oxide: evolutionary implications, Proc. Natl. Acad. Sci. U.S.A. 96 (1999) 14718–14723.
[10] Y. Huang, J. Reimann, H. Lepp, N. Drici, P. Ädelroth, Vectorial proton transfer coupled to reduction of O_2 and NO by a heme–copper oxidase, Proc. Natl. Acad. Sci. U. S. A. 105 (2008) 20257–20262.
[11] E. Forte, A. Urbani, M. Saraste, P. Sarti, M. Brunori, A. Giuffre, The cytochrome cbb_3 from *Pseudomonas stutzeri* displays nitric oxide reductase activity, Eur. J. Biochem. 268 (2001) 6486–6491.
[12] M.F. Anjum, T.M. Stevanin, R.C. Read, J.W. Moir, Nitric oxide metabolism in *Neisseria meningitidis*, J. Bacteriol. 184 (2002) 2987–2993.
[13] S. Lissenden, S. Mohan, T. Overton, T. Regan, H. Crooke, J.A. Cardinale, T.C. Householder, P. Adams, C.D. O'Conner, V.L. Clark, H. Smith, J.A. Cole, Identification of transcription activators that regulate gonococcal adaptation from aerobic to anaerobic or oxygen-limited growth, Mol. Microbiol. 37 (2000) 839–855.
[14] J. Abramson, S. Riistama, G. Larsson, A. Jasaitis, M. Svensson-Ek, L. Laakkonen, A. Puustinen, S. Iwata, M. Wikström, The structure of the ubiquinol oxidase from *Escherichia coli* and its ubiquinone binding site, Nat. Struct. Biol. 7 (2000) 910–917.
[15] S. Buschmann, E. Warkentin, H. Xie, J.D. Langer, U. Ermler, H. Michel, The structure of cbb_3 cytochrome oxidase provides insights into proton pumping, Science 329 (2010) 327–330.
[16] S. Iwata, C. Ostermeier, B. Ludwig, H. Michel, Structure at 2.8 Å resolution of cytochrome *c* oxidase from *Paracoccus denitrificans*, Nature 376 (1995) 660–669.
[17] T. Soulimane, G. Buse, G.P. Bourenkov, H.D. Bartunik, R. Huber, M.E. Than, Structure and mechanism of the aberrant ba_3-cytochrome *c* oxidase from *Thermus thermophilus*, EMBO J. 19 (2000) 1766–1776.
[18] M. Svensson-Ek, J. Abramson, G. Larsson, S. Törnroth, P. Brzezinski, S. Iwata, The X-ray crystal structures of wild-type and EQ(I-286) mutant cytochrome *c* oxidases from *Rhodobacter sphaeroides*, J. Mol. Biol. 321 (2002) 329–339.
[19] T. Tsukihara, H. Aoyama, E. Yamashita, T. Tomizaki, H. Yamaguchi, K. Shinzawa-Itoh, R. Nakashima, R. Yaono, S. Yoshikawa, The whole structure of the 13-subunit oxidized cytochrome *c* oxidase at 2.8 Å, Science 272 (1996) 1136–1144.
[20] W.H. Woodruff, R.B. Dyer, Ó. Einarsdóttir, Spectroscopy, dynamics, and function of cytochrome oxidase, in: R.J.H. Clark, R.E. Hester (Eds.), Biological Spectroscopy, Part B, John Wiley and Sons Ltd, Chichester, England, 1993, pp. 189–233.
[21] Q.H. Gibson, C. Greenwood, Reactions of cytochrome oxidase with oxygen and carbon monoxide, Biochem. J. 86 (1963) 541–554.
[22] J.O. Alben, P.P. Moh, F.G. Fiamingo, R.A. Altschuld, Cytochrome oxidase (a_3) heme and copper observed by low-temperature Fourier transform infrared spectroscopy of the CO complex, Proc. Natl. Acad. Sci. U.S. A. 78 (1981) 234–237.
[23] R.B. Dyer, Ó. Einarsdóttir, P.M. Killough, J.J. López-Garriga, W.H. Woodruff, Transient binding of photodissociated CO to Cu_B^+ of eukaryotic cytochrome oxidase at ambient temperature. Direct evidence from time-resolved infrared spectroscopy, J. Am. Chem. Soc. 111 (1989) 7657–7659.
[24] Ó. Einarsdóttir, R.B. Dyer, D.D. Lemon, P.M. Killough, S.M. Hubig, S.J. Atherton, J.J. López-Garriga, G. Palmer, W.H. Woodruff, Photodissociation and recombination of carbonmonoxy cytochrome oxidase: dynamics from picoseconds to kiloseconds, Biochemistry 32 (1993) 12013–12024.
[25] Ó. Einarsdóttir, P.M. Killough, J.A. Fee, W.H. Woodruff, An infrared study of the binding and photodissociation of carbonmonoxide in cytochrome ba_3 from *Thermus thermophilus*, J. Biol. Chem. 264 (1989) 2405–2408.
[26] K. Koutsoupakis, S. Stavrakis, E. Pinakoulaki, T. Soulimane, C. Varotsis, Observation of the equilibrium Cu_B–CO complex and functional implications of the transient heme a_3 propionates in cytochrome ba_3-CO from *Thermus thermophilus*. Fourier transform infrared (FTIR) and time-resolved step-scan FTIR studies, J. Biol. Chem. 277 (2002) 32860–32866.
[27] R.S. Blackmore, C. Greenwood, Q.H. Gibson, Studies of the primary oxygen intermediate in the reaction of fully reduced cytochrome oxidase, J. Biol. Chem. 266 (1991) 19245–19249.
[28] E. Pilet, W. Nitschke, F. Rappaport, T. Soulimane, J.C. Lambry, U. Liebl, M.H. Vos, NO binding and dynamics in reduced heme–copper oxidases aa_3 from *Paracoccus denitrificans* and ba_3 from *Thermus thermophilus*, Biochemistry 43 (2004) 14118–14127.
[29] E. Pilet, W. Nitschke, U. Liebl, M.H. Vos, Accommodation of NO in the active site of mammalian and bacterial cytochrome *c* oxidase aa_3, Biochim. Biophys. Acta 1767 (2007) 387–392.
[30] R. MacArthur, A. Sucheta, F.S. Chong, Ó. Einarsdóttir, Photodissociation of a (μ-peroxo)(μ-hydroxo)bis[bis(bipyridyl)cobalt(III)] complex: a tool to study fast biological reactions involving O_2, Proc. Natl. Acad. Sci. U. S. A. 92 (1995) 8105–8109.
[31] N. Van Eps, I. Szundi, Ó. Einarsdóttir, A new approach to study fast biological reactions involving dioxygen: the reaction of fully reduced cytochrome *c* oxidase with O_2, Biochemistry 39 (2000) 14576–14582.
[32] I. Szundi, C. Funatogawa, J.A. Fee, T. Soulimane, Ó. Einarsdóttir, CO impedes superfast O_2 binding in ba_3 cytochrome oxidase from *Thermus thermophilus*, Proc. Natl. Acad. Sci. U. S. A. 107 (2010) 21010–21015.
[33] K.E. Georgiadis, N.-I. Jhon, Ó. Einarsdóttir, Time-resolved optical absorption studies of intramolecular electron transfer in cytochrome *c* oxidase, Biochemistry 33 (1994) 9245–9256.
[34] S.J. Hug, J.W. Lewis, C.M. Einterz, T.E. Thorgeirsson, D.S. Kliger, Nanosecond photolysis of rhodopsin: evidence for a new, blue-shifted intermediate, Biochemistry 29 (1990) 1475–1485.
[35] I. Szundi, J.W. Lewis, D.S. Kliger, Deriving reaction mechanisms from kinetic spectroscopy. Application to late rhodopsin intermediates, Biophys. J. 73 (1997) 688–702.
[36] I. Szundi, N. Van Eps, Ó. Einarsdóttir, pH dependence of the reduction of dioxygen to water by cytochrome *c* oxidase. 2. Branched electron transfer pathways linked by proton transfer, Biochemistry 42 (2003) 5074–5090.
[37] R.B. Dyer, K.A. Peterson, P.O. Stoutland, W.H. Woodruff, Picosecond infrared study of the photodynamics of carbonmonoxy-cytochrome *c* oxidase, Biochemistry 33 (1994) 500–507.
[38] T. Hayashi, M.T. Lin, K. Ganesan, Y. Chen, J.A. Fee, R.B. Gennis, P. Moenne-Loccoz, Accommodation of two diatomic molecules in cytochrome *bo*: insights into NO reductase activity in terminal oxidases, Biochemistry 48 (2009) 883–890.

[39] L.M. Hunsicker-Wang, R.L. Pacoma, Y. Chen, J.A. Fee, C.D. Stout, A novel cryoprotection scheme for enhancing the diffraction of crystals of recombinant cytochrome ba_3 oxidase from *Thermus thermophilus*, Acta Crystallogr. D61 (2005) 340–343.
[40] B. Liu, Y. Chen, T. Doukov, S.M. Soltis, C.D. Stout, J.A. Fee, Combined microspectrophotometric and crystallographic examination of chemically reduced and X-ray radiation-reduced forms of cytochrome ba_3 oxidase from *Thermus thermophilus*: structure of the reduced form of the enzyme, Biochemistry 48 (2009) 820–826.
[41] L.M. Blomberg, M.R. Blomberg, P.E. Siegbahn, A theoretical study on nitric oxide reductase activity in a ba_3-type heme–copper oxidase, Biochim. Biophys. Acta 1757 (2006) 31–46.
[42] C. Koutsoupakis, T. Soulimane, C. Varotsis, Ligand binding in a docking site of cytochrome *c* oxidase: a time-resolved step-scan Fourier transform infrared study, J. Am. Chem. Soc. 125 (2003) 14728–14732.
[43] E. Pinakoulaki, H. Yoshimura, V. Daskalakis, S. Yoshioka, S. Aono, C. Varotsis, Two ligand-binding sites in the O_2-sensing signal transducer HemAT: implications for ligand recognition/discrimination and signaling, Proc. Natl. Acad. Sci. U. S. A. 103 (2006) 14796–14801.
[44] K. Muramoto, K. Ohta, K. Shinzawa-Itoh, K. Kanda, M. Taniguchi, H. Nabekura, E. Yamashita, T. Tsukihara, S. Yoshikawa, Bovine cytochrome *c* oxidase structures enable O_2 reduction with minimization of reactive oxygens and provide a proton-pumping gate, Proc. Natl. Acad. Sci. U.S.A. 107 (2010) 7740–7745.
[45] K. Ohta, K. Muramoto, K. Shinzawa-Itoh, E. Yamashita, S. Yoshikawa, T. Tsukihara, X-ray structure of the NO-bound Cu_B in bovine cytochrome c oxidase, Acta Crystallogr. Sect. F Struct. Biol. Cryst. Commun. 66 (2010) 251–253.
[46] R.B. Dyer, J.J. López-Garriga, Ó. Einarsdóttir, W.H. Woodruff, The orientation of CO in carbonmonoxy cytochrome oxidase and its transient photoproducts. Direct evidence from time-resolved infrared linear dichroism, J. Am. Chem. Soc. 111 (1989) 8962–8963.
[47] S.A. Siletsky, I. Belevich, A. Jasaitis, A.A. Konstantinov, M. Wikström, T. Soulimane, M.I. Verkhovsky, Time-resolved single-turnover of ba_3 oxidase from *Thermus thermophilus*, Biochim. Biophys. Acta 1767 (2007) 1383–1392.
[48] R.A. Goldbeck, Ó. Einarsdóttir, T.D. Dawes, D.B. O'Connor, K.K. Surerus, J.A. Fee, D.S. Kliger, Magnetic circular dichroism study of cytochrome ba_3 from *Thermus thermophilus*: Spectral contributions from cytochromes *b* and a_3 and nanosecond spectroscopy of CO photodissociation intermediates, Biochemistry 31 (1992) 9376–9387.
[49] V.M. Luna, Y. Chen, J.A. Fee, C.D. Stout, Crystallographic studies of Xe and Kr binding within the large internal cavity of cytochrome ba_3 from *Thermus thermophilus:* structural analysis and role of oxygen transport channels in the heme–Cu oxidases, Biochemistry 47 (2008) 4657–4665.
[50] L. Salomonsson, A. Lee, R.B. Gennis, P. Brzezinski, A single-amino-acid lid renders a gas-tight compartment within a membrane-bound transporter, Proc. Natl. Acad. Sci. U. S. A. 101 (2004) 11617–11621.
[51] A. Giuffrè, E. Forte, G. Antonini, E. D'Itri, M. Brunori, T. Soulimane, G. Buse, Kinetic properties of ba_3 oxidase from *Thermus thermophilus*: effect of temperature, Biochemistry 38 (1999) 1057–1065.
[52] I.A. Smirnova, D. Zaslavsky, J.A. Fee, R.B. Gennis, P. Brzezinski, Electron and proton transfer in the ba_3 oxidase from *Thermus thermophilus*, J. Bioenerg. Biomembr. 40 (2008) 281–287.
[53] Ó. Einarsdóttir, I. Szundi, Time-resolved optical absorption studies of cytochrome oxidase dynamics, Biochim. Biophys. Acta 1655 (2004) 263–273.
[54] N. Van Eps, I. Szundi, Ó. Einarsdóttir, pH dependence of the reduction of dioxygen to water by cytochrome *c* oxidase. 1. The P_R state is a pH-dependent mixture of three intermediates, A, P, and F, Biochemistry 42 (2003) 5065–5073.
[55] M. Karpefors, P. Ädelroth, A. Aagaard, H. Sigurdson, M. Svensson-Ek, P. Brzezinski, Electron–proton interactions in terminal oxidases, Biochim. Biophys. Acta 1365 (1998) 159–169.
[56] A. Sucheta, I. Szundi, Ó. Einarsdóttir, Intermediates in the reaction of fully reduced cytochrome *c* oxidase with dioxygen, Biochemistry 37 (1998) 17905–17914.
[57] M.I. Verkhovsky, J.E. Morgan, M. Wikström, Oxygen binding and activation: early steps in the reaction of oxygen with cytochrome *c* oxidase, Biochemistry 33 (1994) 3079–3086.